Nuclear Physics B292 (1987) 745–766
North-Holland, Amsterdam

K^0–$\bar{K}^0$ MIXING AT THREE LOOPS
Short-distance double penguin-like diagrams

J.O. EEG

Institute of Physics, University of Oslo, Oslo, Norway

I. PICEK*

DESY, Hamburg, Federal Republic of Germany

Received 30 October 1986
(Revised 26 January 1987)

We consider diagrams of order $\alpha_s^2 G_F^2$ for the K^0–$\bar{K}^0$ mixing, topologically different from the gluon-corrected standard box. The treatment of three-loop diagrams is simplified by factorizing them in terms of momentum-dependent effective vertices for $s \to dG$ and $s \to dGG$ transitions. An enhancement from the remaining loop-momentum integration compensates for the extra powers of the strong coupling. This gives a significant contribution to the *CP*-violating part (-15% to -40% of the standard-box value). The dependence of the results on the involved mass parameters is illustrated by LEGO plots for both the *CP*-conserving and *CP*-violating parts.

1. Introduction

The K^0–$\bar{K}^0$ mixing represents an exquisitely sensitive test both for the minimal standard model (SM) and its possible extensions. The extremely small $K_L - K_S$ mass difference

$$\Delta m_K^{\exp} \simeq 3.5 \times 10^{-15}\ \text{GeV} \tag{1.1}$$

requires the effective $\Delta S = 2$ interaction producing it to be $O(G_F^2)$. Indeed, in the lowest-order interaction in G_F, the SM provides only the $\Delta S = 0, 1$ transitions, and the first modern treatment of the $\Delta S = 2$ transition was represented by the calculation of the box-loop diagram (fig. 1) by Gaillard and Lee [1]. This calculation also nicely exhibited the GIM cancellation [2] operating at the one-loop level and led to the prediction of the charmed-quark mass. However, the most critical test of the SM seems to reside in the explanation of *CP* violation. The only observed *CP*-violating quantity is still the parameter ε of the K^0–$\bar{K}^0$ system,

$$\varepsilon \simeq 2.27 \times 10^{-3}. \tag{1.2}$$

* A. von Humboldt fellow, on leave of absence from the Rudjer Bošković Institute, Zagreb, Croatia, Yugoslavia. Supported in part by the JFP-683/NSF grant.

0550-3213/87/$03.50 © Elsevier Science Publishers B.V.
(North-Holland Physics Publishing Division)

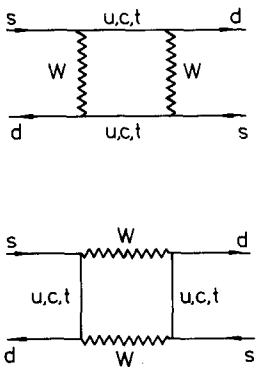

Fig. 1. Scattering and annihilation channels of the standard-box diagram.

In the minimal SM, *CP* violation appears only as a loop effect and, in addition, represents the single low-energy amplitude given by the high mass scale (of the third generation of fermions). If there exist new interactions, these should influence the sensitive $O(G_F^2)$ quantities (1.1) and (1.2). Thus, the quantities (1.1) and (1.2) lead to bounds on various "beyond the SM" models: the extension by a fourth generation of quarks [3], left-right symmetric theories [4], supersymmetric theories [5], extra Higgs bosons [6], composite models [7] and even Lorentz non-invariant couplings [8].

From the theoretical point of view, the extreme experimental precision of (1.1) and the uniqueness of (1.2) require a very precise computation. Before having precise theoretical values for these quantities, the recent claims of deviations from the standard model seem to be premature. However, there is a well-known obstacle in obtaining precise predictions in hadronic physics: it comes from the problem of separating short-distance (SD) from long-distance (LD) dispersive effects [9], and from the theoretical uncertainty in the latter. In order to remedy for this difficulty, we focus on the effects dominated by trustably calculable SD contributions. The effect which we consider here is the imaginary (*CP*-violating) part of the K^0–$\bar{K}^0$ mixing; this part seems to come mainly from the SD effects [10]. In a separate paper we intend to consider the B^0–$\bar{B}^0$ mixing [11], for which the real part (Δm_B) also appears to be SD dominated [12].

The latter effect is interesting in view of the increasing body of data from heavy-quark physics [13]. The progress in this direction has a chance to remove the kaon from the distinguished place of being the only physical system providing a measured *CP* non-invariance.

In this paper we make an attempt to recheck with more accuracy the predictions of the minimal SM for the K^0–$\bar{K}^0$ system. We lay special emphasis on double penguin-like (DPL) diagrams, which have recently been studied with considerable interest [14–18]. These diagrams represent potentially important effects from

higher-order loops. This is because the particular loop integrals under consideration give an enhancement which might compensate for the extra powers of the strong coupling invoked in such diagrams. However, explicit calculations are needed in order to know the importance of such loop effects. A nice feature of such new contributions is that they lead to a local four-quark operator of the same type as the one of the simple box diagram. Thus, the ratio of the DPL matrix element to the standard-box matrix element is free of ambiguities. However, the well-known ambiguity (phrased as the "B factor" [19]) enters when we want to know the net value of the new contributions to the experimentally measured quantities (1.1) and (1.2).

The paper is organized as follows. Sect. 2 is the central part of the paper, with subsect. 2.1 restricted to the general properties and the leading approximation form of the three-loop diagrams and subsect. 2.2 exposing the results of numerical evaluation. Details of vertices, approximate analytical results and colour factors are given in appendices A, B and C, respectively. Sect. 3 is devoted to conclusions.

2. Box diagrams of penguin variety

2.1. GENERAL STRUCTURE OF DOUBLE PENGUIN-LIKE DIAGRAMS

In our recent short papers [17, 18] we reported briefly on an additional class of diagrams contributing to the K^0–$\bar{K}^0$ mixing. Their importance was measured in a ratio to the standard box. In our first paper [17] we resolved the "double penguin" controversy raised by papers [14, 16] and [15] concerning the importance of a particular class of double penguin (DP) diagrams (fig. 2) for the mass difference

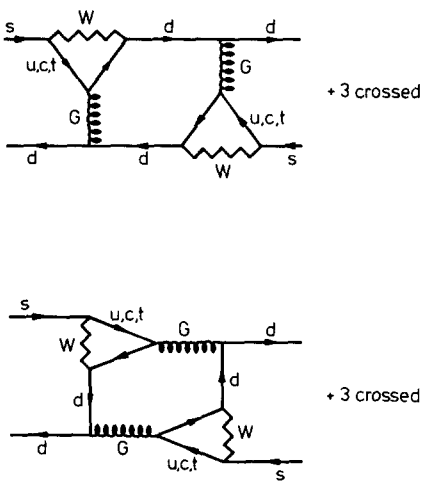

Fig. 2. Original double-penguin diagram, its annihilation-channel counterpart and indication of their crossed diagram companions.

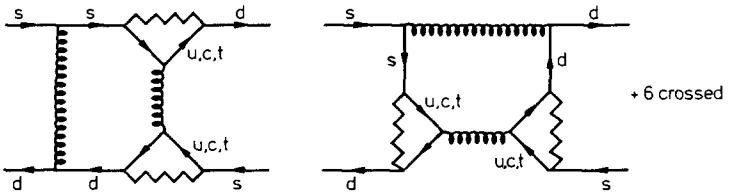

Fig. 3. Siamese-penguin diagrams, here as a first example of the QCD gauge-dependent extension of double penguins.

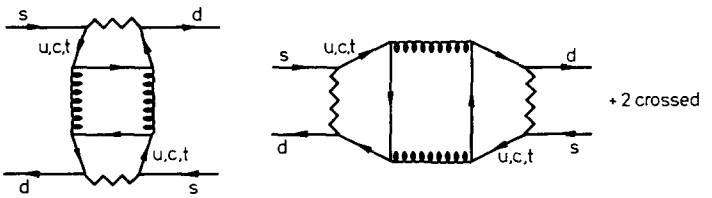

Fig. 4. Diamond box, another gauge-dependent diagram of order $\alpha_s^2 G_F^2$.

(1.1): the new contribution to Δm_K, being of the order of one percent, was entirely negligible. In our second paper [16] we considered a full class of double penguin-like (DPL) box diagrams of order $\alpha_s^2 G_F^2$. As well as the original DP there is a "siamese penguin" (SP) box (fig. 3), a "diamond" (D) box (fig. 4) and a "mixed penguin" (MP) box (fig. 5). As a result we obtained (for some average choice of the parameters involved) that such a new contribution to the *CP*-violating parameter ε (eq. (1.2)) constitutes approximately -25% of the standard-box value. The present paper is intended to have a wider scope. As well as giving a detailed presentation of the calculation, we also investigate the stability and (for a reasonable range of parameters) the range of the new *CP*-conserving and *CP*-violating parts of the K^0–$\bar{K}^0$ mixing.

The vertices appearing in the diagrams of figs. 2–5 include not only the ordinary flavour-conserving gluon vertex, but also the induced flavour-changing vertices

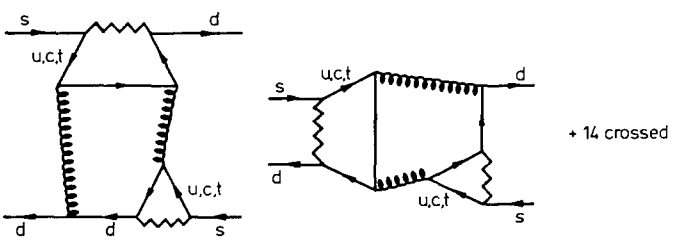

Fig. 5. Mixed-penguin diagrams, representing the largest subclass under consideration.

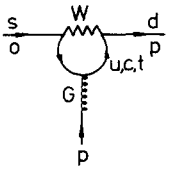

Fig. 6. Induced flavour changing s → dG (penguin) vertex (given in (A.2)–(A.4)).

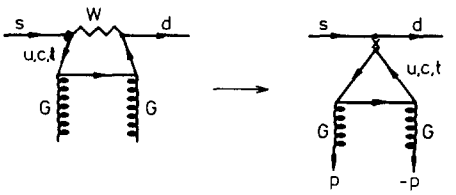

Fig. 7. s → dGG penguin vertex, reducing to a triangle anomaly vertex for the heavy W-boson (given in (A.6)–(A.14)).

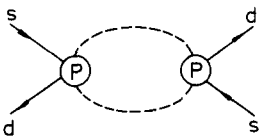

Fig. 8. A schematic presentation of the momentum-dependent penguin-type vertices entering a common loop-momentum integration. The dashed line represents a quark or a gluon.

s → dG and s → dGG (figs. 6 and 7). We list them systematically in a separate appendix (app. A). The diagrams at hand are apparently complicated three-loop diagrams. However, they can be considerably simplified by neglecting the external quark momenta for the kaon system* and by factorizing the loop integration into the momentum-dependent effective vertices and a common loop-momentum integration, as shown schematically in fig. 8. In such a treatment we insert the QCD running coupling $\alpha_s(p^2)$ under the loop integrals, as inspired by previous loop calculations [21, 22].

Let us explain our evaluation of loops in more detail by using the example of the double penguin displayed in fig. 2. The relevant s → dG vertex is represented by a sum of "single" quark contributions L_q (q = u, c, t) (eq(A.5)):

$$\lambda_u L_u + \lambda_c L_c + \lambda_t L_t , \tag{2.1}$$

where

$$\lambda_q = V_{qd} V_{qs}^* .$$

* The external mass effect for the standard box has recently been considered by Datta and Kumbhakar [20].

Since the Kobayashi-Maskawa (KM) factors are constrained by the relation

$$\lambda_u + \lambda_c + \lambda_t = 0, \tag{2.2}$$

eq. (2.1) can be cast into the form

$$\lambda_u [L_u - L_c] - \lambda_t [L_c - L_t]. \tag{2.3}$$

This relation representing the GIM cancellation mechanism leads to the expression

$$f_P(p^2) C_P(p^2, m^2, M^2)\, \bar{d}\gamma_\alpha t^a L s P_T(p)^\alpha_\rho, \tag{2.4a}$$

where

$$C_P(p^2, m^2, M^2) = 6\int_0^1 \mathrm{d}x\, x(1-x) \ln \frac{M^2 + p^2 x(1-x)}{m^2 + p^2 x(1-x)}, \tag{2.4b}$$

and $f_P \sim G_F g_s$ is defined in (A.3). In eq. (2.4b), (m, M) refers to either the (m_u, m_c) or (m_c, m_t) pair of current quark masses.

Attaching to this vertex the accompanying gluon propagator results in an effective penguin vertex which is QCD gauge independent:

$$P_T(p)^\alpha_\rho D_G(p)^{\rho\beta} = P_T(p)^\alpha_\rho \frac{1}{p^2}\left[g^{\rho\beta} - \xi \frac{p^\rho p^\beta}{p^2} \right] = g^{\alpha\beta} - \frac{p^\alpha p^\beta}{p^2}. \tag{2.5}$$

When the external quark momenta are neglected, such a vertex enters the schematic diagram (fig. 6) already mentioned. Its amplitude is given by a single loop-momentum integration

$$\int \frac{\mathrm{d}^4 p}{(2\pi)^4} [f_P(p^2)]^2 \left(\bar{d}\gamma_\mu t^a S_d(-p)\gamma_\beta t^b L s\right) P_T(p)^\beta_\alpha D_G(p)^{\alpha\sigma}$$

$$\times C_P(p^2)_1 \left(\bar{d}\gamma_\sigma t^b S_{\bar{d}}(-p)\gamma_\lambda t^a L s\right) P_T(p)^\lambda_\nu D_G(p)^{\nu\mu} C_P(p^2)_2, \tag{2.6a}$$

where

$$C_P(p^2)_i \equiv C_P(p^2, m_i^2, M_i^2). \tag{2.6b}$$

Among the terms resulting from the insertion of (2.5) in (2.6) we choose those involving the second term ("non-local" part of the penguin) in the r.h.s. of eq. (2.5). These terms introduce loop integrals involving extra four momenta in the numerator. In our case (neglecting external momenta), such terms can be easily handled by making replacements such as $p_\mu p_\nu \to \frac{1}{4} p^2 g_{\mu\nu}$ (app. B of ref. [23]). Then such loop

integrals reduce to the expressions proportional to the "local" contribution of the penguin:

$$\frac{1}{36}\int\frac{d^4p}{(2\pi)^4}\frac{1}{p^2}C_P(p^2)_1C_P(p^2)_2. \tag{2.7}$$

As shown in our previous paper [17], inclusion of the "non-local" parts for the DP diagrams effectively gave a minus sign (the factor $-\frac{15}{16}$) to the purely "local" part treated in ref. [14]. In contrast to [14], we conclude that the pure DP-diagram contribution to Δm_K was negligible in comparison with the standard box contribution. Still we conjectured about the possible new contributions to the *CP*-violating parameter ε. A realization of this conjecture was demonstrated in our subsequent paper [18]. In contrast to the DP box, the additional diagrams in figs. 3–5 are not gauge independent by themselves. In order to show that the diagrams in figs. 3–5 complete to a gauge-invariant set, we have expressed their explicit contribution in the leading log approximation as*

$$\tilde{M}_{\text{l-log}} = \left(\bar{d}\gamma_\mu Ls\right)^2\left(2\sqrt{2}\,G_F\right)^2\frac{1}{16\pi^2}\int dp^2\left(\frac{\alpha_s(p^2)}{4\pi}\right)^2\left(\ln\frac{M^2}{p^2}\right)^2. \tag{2.8}$$

Here the colour and Dirac-algebra factors are already extracted. Then, as shown in (2.5), the DP is gauge independent by itself

$$M^{DP}_{\text{l-log}} = -\tfrac{68}{27}\tilde{M}_{\text{l-log}}, \tag{2.9}$$

while the rest, namely the gauge-dependent siamese penguin

$$M^{SP}_{\text{l-log}} = \left(-\tfrac{32}{27} - \tfrac{4}{3}\xi\right)\tilde{M}_{\text{l-log}}, \tag{2.10}$$

the diamond box

$$M^{D}_{\text{l-log}} = \left(4 - \tfrac{4}{3}\xi\right)\tilde{M}_{\text{l-log}} \tag{2.11}$$

and the mixed-penguin box

$$M^{MP}_{\text{l-log}} = \left(-8 + \tfrac{8}{3}\xi\right)\tilde{M}_{\text{l-log}}, \tag{2.12}$$

obviously add up to a gauge-invariant result. However, the l-log expressions cannot account for the dominating *CP*-violating part (the interference *K*-term defined later). Thus we find the analytical expressions which give the interference *CP*-violating term $\sim\lambda_u\lambda_t$ in the leading approximation, for which $(L_c - L_t) \sim \ln(m_t^2/p^2)$

* In eq. (2.8) we have used "l-log" to denote l-log for individual penguin loops. This does not mean that the total integral in (2.8) is leading log (after integration over p^2).

and $(L_u - L_c) \sim m_c^2/p^2$ in the region $m_c^2 < p^2 < m_t^2$. We obtain the following total (crossed plus uncrossed diagrams, scattering and annihilation channel included) DP, SP, D and MP contributions:

$$M^{\mathrm{DP}}_{\text{next-lead}} = -\tfrac{68}{27} 6R\langle Q\rangle, \tag{2.9a}$$

$$M^{\mathrm{SP}}_{\text{next-lead}} = \left(-\tfrac{32}{27} - \tfrac{4}{3}\xi\right) 6R\langle Q\rangle, \tag{2.10a}$$

$$M^{\mathrm{D}}_{\text{next-lead}} = 8R(1-\xi)\langle Q\rangle, \tag{2.11a}$$

$$M^{\mathrm{MP}}_{\text{next-lead}} = -8\left[(4-2\xi)R + \tfrac{13}{18}(S-R)\right]\langle Q\rangle, \tag{2.12a}$$

where R, S and $\langle Q\rangle$ are defined in appendix B. This approximation for $m_c^2 < p^2 < m_t^2$ could be called "next to leading", in contrast to the "leading-log" approximation in (2.8)–(2.12). Then we can demonstrate the gauge independence of the dominating *CP*-violating part in this next-to-leading approximation. Beyond the approximations in (2.9)–(2.12) and (2.9a)–(2.12a) it is not so trivial to show the gauge independence of the sum of *all diagrams* explicitly. For instance, some additional non-leading diagrams involving the self-energy $s \to d$ transitions complicates the theoretical analysis.

In appendix B we also give the approximate analytical results for the dominating *CP*-violating *K*-integrals. In spite of the crudeness of this approximation, the obtained results agree within a factor of two with the numerical integration done in the rest of the paper. The obtained analytical expressions may therefore give some insight in the variation of the *K*-integrals, discussed later.

Once we have proved the QCD gauge independence at some leading level, we calculate the individual DPL-box contributions beyond the leading (log) order in the Feynman gauge ($\xi = 0$ in eq. (2.5)). For the DP box, relations (2.8) and (2.9) and the corresponding relation (2.9a) get replaced by the full expression*

$$M^{\mathrm{DP}} = -\frac{68}{27}\left(\frac{2\sqrt{2}\,G_F}{16\pi^2}\right)^2 \left\{\int \mathrm{d}p^2 \left[\alpha_s(p^2)\right]^2 C_P(p^2)_1 C_P(p^2)_2\right\} \left(\bar{d}\gamma_\mu Ls\right)^2. \tag{2.13}$$

Thus far we have considered our second reference point, namely the DP boxes. Similar expressions for the other boxes of penguin variety are given by replacing the appropriate one-gluon vertices (2.4) by the corresponding two-gluon vertices (A.6).

* This expression takes into account colour factors which are different for scattering and annihilation channels. Details of the colour factors are explained in app. C.

The SP box is given by the same loop-momentum integral as the DP box:

$$M^{\mathrm{SP}} = -\frac{32}{27}\left(\frac{2\sqrt{2}\,G_{\mathrm{F}}}{16\pi^2}\right)^2\left\{\int \mathrm{d}p^2\,[\alpha_{\mathrm{s}}(p^2)]^2 C_{\mathrm{P}}(p^2)_1 C_{\mathrm{P}}(p^2)_2\right\}(\bar{d}\gamma_\mu Ls)^2. \quad (2.14)$$

The amplitude of the diamond box displayed in fig. 4 has the form determined by (A.6–11):

$$\int \frac{\mathrm{d}^4p}{(2\pi)^4}[f_{\mathrm{T}}(p^2)]^2(\bar{d}\gamma^\mu Lt^b t^a s)T_{\mu\sigma\rho}(p^2)D_{\mathrm{G}}(p)^{\beta\rho}$$

$$\times D_{\mathrm{G}}(p)^{\alpha\sigma}T_{\nu\beta\alpha}(p^2)(\bar{d}\gamma^\nu Lt^a t^b s), \quad (2.15)$$

and there are similar expressions for the crossed diagrams. In eq. (2.15), f_{T} is of order $G_{\mathrm{F}}\alpha_{\mathrm{s}}$ [(A.7)], while the tensor $T_{\alpha\rho\sigma}$ consists of a symmetric and an antisymmetric part:

$$T_{\alpha\rho\sigma} = T^{\mathrm{S}}_{\alpha\rho\sigma} + T^{\mathrm{A}}_{\alpha\rho\sigma}, \quad (2.16)$$

where

$$T^{\mathrm{S}}_{\mu\rho\sigma} = A(p^2, m^2)[g_{\mu\rho}p_\sigma + g_{\mu\sigma}p_\rho]$$

$$+ B(p^2, m^2)g_{\rho\sigma}p_\mu + C(p^2, m^2)p_\mu p_\rho p_\sigma, \quad (2.17a)$$

$$T^{\mathrm{A}}_{\mu\rho\sigma} = -iF(p^2, m^2)\varepsilon_{\mu\rho\sigma\tau}p^\tau. \quad (2.17b)$$

After the extraction of the colour part of the D matrix element, the crossed and uncrossed diagrams give (see the last footnote)

$$M^{\mathrm{D}} = \left(\frac{2\sqrt{2}\,G_{\mathrm{F}}}{16\pi^2}\right)^2\int \mathrm{d}p^2\,[\alpha_{\mathrm{s}}(p^2)]^2\{2[6A(p^2)_1A(p^2)_2 + 3B(p^2)_1B(p^2)_2$$

$$+ (2A(p^2)_1 + B(p^2)_1 - p^2C(p^2)_1)(2A(p^2)_2 + B(p^2)_2 - p^2C(p^2)_2)]$$

$$- \tfrac{52}{3}F(p^2)_1F(p^2)_2\}(\bar{d}\gamma_\mu Ls)^2. \quad (2.18)$$

Finally, the MP amplitude for the diagram displayed in fig. 5 is

$$\int \frac{\mathrm{d}^4p}{(2\pi)^4}g_{\mathrm{s}}(p^2)f_{\mathrm{P}}(p^2)f_{\mathrm{T}}(p^2)(\bar{d}\gamma_\mu Lt^b t^a s)C_{\mathrm{P}}(p^2)_1 D_{\mathrm{G}}(p)^{\beta\rho}D_{\mathrm{G}}(p)^{\sigma\alpha}$$

$$\times P_{\mathrm{T}}(p)_{\nu\alpha}T_{\mu\sigma\rho}(p^2)_2[\bar{d}\gamma_\beta t^a S_{\bar{d}}(-p)\gamma^\nu Lt^b s], \quad (2.19)$$

and there are similar expressions for the crossed diagrams. As may be inferred from their name, these diagrams are determined by different vertices from appendix A. Summed up, after the extraction of the colour factors they give

$$M^{\mathrm{MP}} = \left(\frac{2\sqrt{2}\,G_{\mathrm{F}}}{16\pi^2}\right)^2 \int \mathrm{d}p^2\,[\alpha_{\mathrm{s}}(p^2)]^2 4\{[A(p^2)_1 - B(p^2)_1 - \tfrac{26}{9}F(p^2)_1]C_{\mathrm{P}}(p^2)_2$$

$$+ C_{\mathrm{P}}(p^2)_1[A(p^2)_2 - B(p^2)_2 - \tfrac{26}{9}F(p^2)_2]\}(\bar{d}\gamma_\mu Ls)^2. \tag{2.20}$$

Now, we return to the schematic diagram in fig. 6. This diagram gives the K^0–$\overline{\mathrm{K}}^0$ mixing matrix element basically determined by a square of eq. (2.3), and has the form

$$\lambda_{\mathrm{u}}^2 I(\mu^2, m_{\mathrm{c}}^2) - 2\lambda_{\mathrm{u}}\lambda_{\mathrm{t}} K(\mu^2, m_{\mathrm{t}}^2) + \lambda_{\mathrm{t}}^2 I(m_{\mathrm{c}}^2, m_{\mathrm{t}}^2). \tag{2.21}$$

Each of the DPL boxes discussed above gives its own contribution to the three terms in eq. (2.21). Using the conventional choice of the KM matrix (where λ_{u} is purely real), we refer to these three terms as *CP*-conserving, *CP*-violating and KM-suppressed *CP*-violating terms, respectively. The terms contain an indication about the range of the loop momentum. Obviously, for $I(\mu^2, m_{\mathrm{c}}^2)$ and $I(m_{\mathrm{c}}^2, m_{\mathrm{t}}^2)$, this range is given by the GIM mechanism [eq. (2.3)], while $K(\mu^2, m_{\mathrm{t}}^2)$ represents an interference term. Note that in eq. (2.21) we have introduced an infrared (IR) cut-off μ in order to make the perturbative evaluation sensible. Thus μ is defined by a critical value of the strong coupling,

$$\alpha_{\mathrm{s}}(\mu^2) = 1. \tag{2.22}$$

The form of the strong running coupling used to evaluate the loops at $p^2 < M^2$ is

$$\alpha_{\mathrm{s}}(p^2) = \alpha_{\mathrm{s}}(M^2) \Big/ \left\{1 - b\frac{\alpha_{\mathrm{s}}(M^2)}{4\pi}\ln\frac{M^2}{p^2}\right\}, \tag{2.23}$$

with $b = 11 - \frac{2}{3}N_f$, where N_f is the effective number of quark flavours.

2.2. RESULTS OF NUMERICAL LOOP EVALUATION

The values of the integrals in (2.21), calculated previously [18] are worth examining in detail. This applies in particular to the *CP*-violating part $K(\mu^2, m_{\mathrm{t}}^2)$, which exceeds the bound up to which the LD contribution could contribute. However, there is an intrinsic uncertainty in our calculation in the form of the IR cut-off μ, reflecting our incapability of performing the non-perturbative calculation in the problem under consideration. *Qualitatively*, the LD contributions to ε, where the virtual process $\mathrm{K}^0 \to \eta^0 \to \overline{\mathrm{K}}^0$ is thought to be most important, are related to the

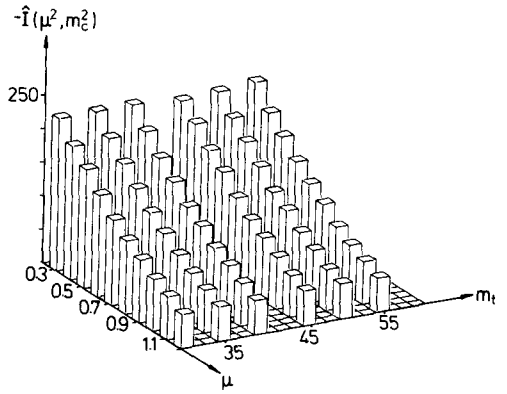

Fig. 9. LEGO plot for a dimensionless integral $\hat{I}(\mu^2, m_c^2)$ relevant for the *CP*-conserving K^0–$\bar{K}^0$ mixing.

uncertainty in the IR cut-off μ. However, the SD perturbative calculation, although dependent on the IR cut-off, can *not* give us information about the LD contribution (by extrapolating the perturbative calculation to the non-perturbative region). The eventual stability of the SD result on the IR cut-off merely indicates that the SD contribution by *itself* is well defined. The perturbative calculation performed requires a numerical treatment of multiple integrals over the loop momentum and the Feynman parameters. For this purpose, we have used the numerical routine VEGAS [24].

In the following we look for the dependence of the evaluated quantities on the variation of μ and the top-quark mass (experimentally not yet determined). The suitable quantities are the dimensionless integrals $\hat{I}(m^2, M^2)$ defined by

$$I(m^2, M^2) = \left[M\alpha_s(M^2)\right]^2 \hat{I}(m^2, M^2), \tag{2.24a}$$

and for convenience

$$K(\mu^2, m_t^2) = \left[m_t\alpha_s(m_t^2)\right]^2 \hat{K}(\mu^2, m_t^2). \tag{2.24b}$$

Their two-dimensional LEGO plots are displayed in figs. 9–11 for μ in a rather wide range, (0.3, 1.2) GeV, and for $m_t \in (30, 55)$ GeV. Since these integrals are fairly stable in m_t, let us focus on their μ dependence (table 1). Obviously, only the *CP*-conserving integral $\hat{I}(\mu^2, m_c^2)$ depends on μ substantially. Furthermore, we may fix μ at some average value to illustrate the relative importance of various DPL diagrams. As seen from table 2, the largest contribution comes from the largest class of MP diagrams (fig. 5) which add up coherently. It is also convenient to express the DPL contributions in terms of their gauge-independent subunit, DP, as shown in

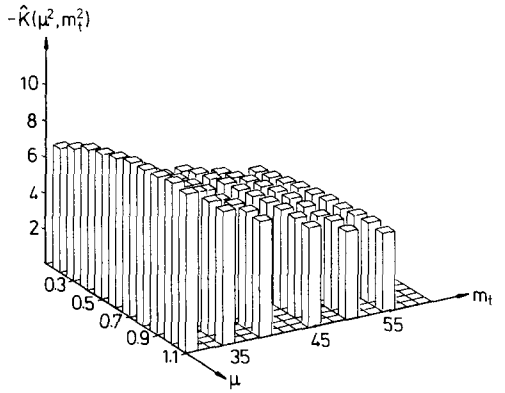

Fig. 10. LEGO plot for a dimensionless integral $\hat{K}(\mu^2, m_t^2)$ relevant for the *CP*-violating K^0–$\overline{K}^0$ mixing.

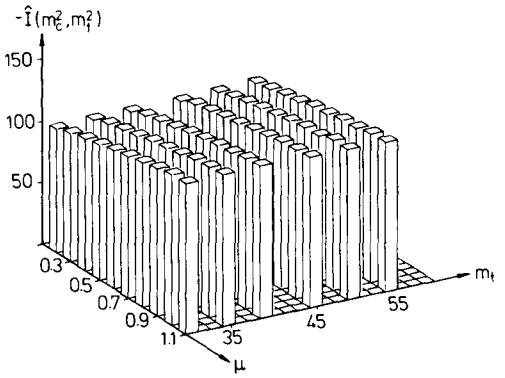

Fig. 11. LEGO plot for a dimensionless integral $\hat{I}(m_c^2, m_t^2)$ relevant for the KM suppressed K^0–$\overline{K}^0$ mixing.

TABLE 1
Range of values of the dimensionless integrals in (2.24) when the IR cut-off is varied in the range (0.3, 1.2) GeV and for fixed $m_t = 45$ GeV

CP-conserving $\hat{I}(\mu^2, m_c^2)$	$(-219.7, -52.1)$
CP-violating $\hat{K}(\mu^2, m_t^2)$	$(-4.2, -5.6)$
CP-violating $\hat{I}(m_c^2, m_t^2)$ suppressed	$(-102.7, -123.5)$

TABLE 2
Separate DPL box-diagram contributions to quantities in table 1, for $\mu = 0.7$ GeV (the colour factors in DP and SP are already extracted)

Loop integral	DPL box	DP	SP	D	MP
$\hat{I}(\mu^2, m_c^2)$		12.9	12.9	15.1	−82.8
$\hat{K}(\mu^2, m_t^2)$		0.6	0.6	0.8	−3.6
$\hat{I}(m_c^2, m_t^2)$		13.3	13.3	21.7	−79

table 3. Then, note that the sum ΣDPL over all new diagrams of order $\alpha_s^2 G_F^2$ gives

$$M^{\mathrm{DPL}} = \frac{G_F^2}{16\pi^2}\left(\frac{2\sqrt{2}}{4\pi}\right)^2 \left\{\lambda_u^2 I(\mu^2, m_c^2) - 2\lambda_u\lambda_t K(\mu^2, m_t^2) + \lambda_t^2 I(m_c^2, m_t^2)\right\}$$

$$\times \left(\bar{d}\gamma_\mu Ls\right)^2_{\mathrm{colourless}}. \tag{2.25}$$

Its separate parts can be directly compared with a QCD-corrected [25] standard-box result, which is numerically as follows:

$$M^{\mathrm{stand.\,box}} = \frac{G_F^2}{16\pi^2}\left\{\lambda_u^2 \times 25.12 - 2\lambda_u\lambda_t \times 61.92\right.$$

$$\left. + \lambda_t^2 \times 19380\right\}\left(\bar{d}\gamma_\mu Ls\right)^2_{\mathrm{colourless}}. \tag{2.26}$$

(The curly bracket is given in the units GeV^2). Eq. (2.26) yields the last column in table 3 (for $m_t = 45$ GeV, $\mu = 0.7$ GeV). However, it is interesting to know how much these percentages vary with the variation of μ^2 and m_t^2. This is shown in table 4 for a fixed value of m_t, $m_t = 45$ GeV (as in table 1) and for the whole range of values of dimensionful integrals (2.24) from figs. 12–14. Thus, the most interesting

TABLE 3
DPL-box contributions from table 2, giving dimensionful quantities according to (2.24); normalized to the DP box and compared with the standard box

	DPL boxes in units of DP					% of the QCD corrected standard box
	DP	SP	D	MP	Σ_{all} DPL	
CP-conserving	1	0.47	−0.46	2.52	3.53	−10%
CP-violating	1	0.47	−0.51	2.45	3.41	−25%
CP-violating suppressed	1	0.47	−0.64	2.32	3.15	−2%

TABLE 4
Range of the net DPL contribution for fixed m_t and for a whole range of values for μ and m_t

	For m_t and μ from table 1		For a whole m_t and μ region from LEGO plots
	the net DPL contribution	% of the standard box	% of the standard box
CP-conserving $I(\mu^2, m_c^2)$	$(-41.9, -68.6)$	$-(8\text{–}14)\%$	$-(8\text{–}14)\%$
CP-violating $K(\mu^2, m_t^2)$	$(-196.4, -445.6)$	$-(16\text{–}36)\%$	$-(13\text{–}39)\%$
CP-violating $I(m_c^2, m_t^2)$ suppressed	$(-4798, -9856)$	$-(1.2\text{–}2.5)\%$	$-(1\text{–}5)\%$

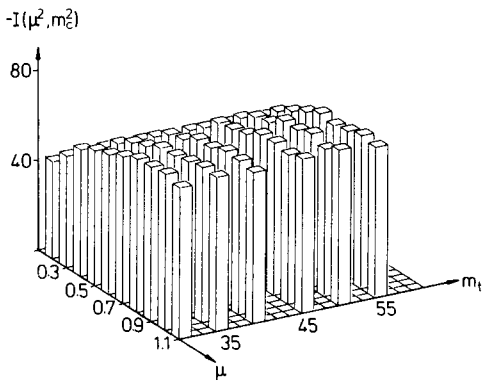

Fig. 12. Dimensionful quantity related to fig. 9 by the relation (2.24). Note that the pattern of fig. 9 changes because of the rapid variation of α_s.

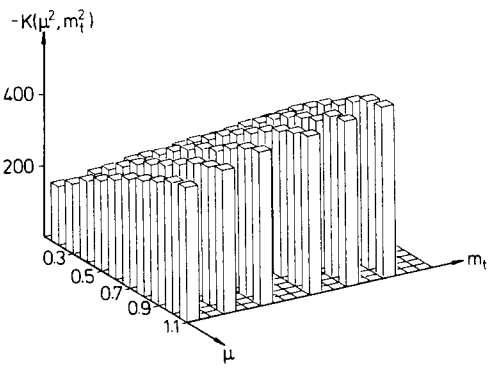

Fig. 13. Dimensionful quantity related to fig. 8.

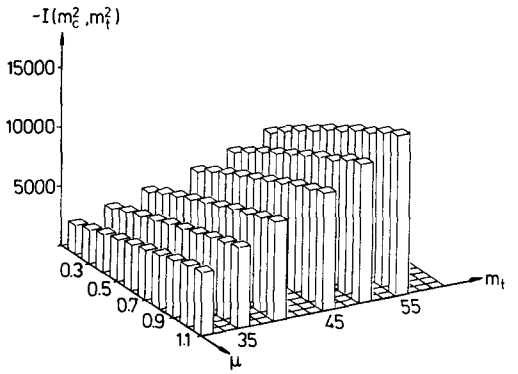

Fig. 14. Dimensionful quantity related to fig. 9.

result

$$-25\% \qquad \text{for } \mu = 0.7 \text{ GeV} \qquad \text{and} \qquad m_t = 45 \text{ GeV},$$

which refers to the *CP*-violating part of the DPL boxes, gets replaced by the interval

$$\text{from } -13\% \text{ to } -39\% \qquad \text{for } \mu \in (0.3, 1.2) \text{ GeV},$$

$$m_t \in (30, 55) \text{ GeV}.$$

Both columns containing percentage in table 4 are presented in order to demonstrate that the variation in m_t for a given range is immaterial. The middle row in table 4 is the most interesting one since the first row is in competition with equally (and even more) important long-distance (dispersive) effects, while the third row, being heavily KM suppressed, cannot compete with the dominant *CP*-violating contribution from the middle row.

3. Discussion and conclusion

The numerical results presented in LEGO plots and tables 1–4 show that the DPL diagrams, although being higher than the standard box by the order of α_s^2, cannot be neglected. The reason for this is twofold. First, DPL diagrams have a topological structure different from that of the standard box and therefore are not included in the QCD-corrected box-graph analysis of Gilman and Wise [25]. Second, the $[\alpha_s(m_t^2)]^2$ factor of the (*CP*-violating) amplitude is compensated for partly owing to the fact that penguin diagrams inserted in higher loops introduce the extra gluon momenta in the numerator which are the loop momenta for the last loop integration. However, the new contributions from DPL diagrams appear to be the most relevant ones for the *CP*-violating part. The reason is that the DPL contribution to Δm_K, although not entirely negligible*, faces the other, even

larger contributions. The most important contribution is the long-distance dispersive contribution, associated with large uncertainties, but generally giving [26]

$$\Delta m_K^{LD} \sim \Delta m_K^{box} \qquad (\sim 10^{-15}\ \text{GeV}).$$

Let us emphasize that there are diagrams corresponding to DPL diagrams which by themselves acquire some LD contribution [15,27].

Furthermore, such LD uncertainties are due to replacing the $\Delta S = 2$ effective interaction by the $(\Delta S = 1)^2$ one, and we distinguish them from the LD uncertainty associated with the evaluation of the B factor. There is also a potentially large correction to the real part of the K^0–$\bar{K}^0$ mixing coming from non-vanishing external quark momenta. For example, the correction due to the non-vanishing external quark mass calculated in ref. [20] constitutes 30% for Δm_K, but is considerably smaller for the imaginary part of the K^0–$\bar{K}^0$ mixing.

Since there is much less uncertainty in the imaginary part of the K^0–$\bar{K}^0$ mixing** our new contributions are more important for the *CP*-violating parameter ε. Even more so in view of the possible "*CP* crisis" of the standard model [29].

Note that the "*CP* crisis" has recently undergone a relaxation [30]. From the experimental point of view, the relaxation is due to the fact that the bound on the ratio $(b \to u)/(b \to c)$ has become less stringent (8% instead of 4% reported previously). From the theoretical point of view, the relaxation is due to the possible value $B \simeq 1$ and not necessarily $\simeq \frac{1}{3}$ (table 6 in Langacker [19]).

However, the "*CP* crisis" announced on the basis of the parameter ε resides in the problem of accommodating the experimental results (1.2) by the standard box alone. Thus, lowering the standard-box value in the range from 15% to 40% obtained here might increase the potential "danger" for the minimal standard model. Still, in our opinion, we cannot point to the crisis of the standard model. Rather, we have illustrated the "crisis" of the precise calculation in contrast to the existing precise measurements of Δm_K and ε. In particular, the fact that the DPL class of diagrams characterized by a single order α_s^2 turns out to be important (when compared with the leading log contribution of the standard box summed to all orders in α_s) indicates that more precise calculations are needed. As well as short-distance effects (of the type considered here) there are also long-distance effects which require still more work to be done (the *B* factor, for example) in order to infer from *CP* violation that some new physics is present in the neutral-kaon system.

We would like to thank B. Guberina and R. Peccei for the helpful comments, to F. Cornet and J. Sola for their valuable help in computational matters, and

* The neglect of the pure DP class [17] was somewhat relaxed by the increase caused by the full set of DPL diagrams [18].

** Here the LD contributions are bounded to be less than 20% [28].

to B. Fanton for correcting the English. One of us (I.P.) would like to thank A. von Humboldt Foundation and R. Peccei for warm hospitality at DESY and to the Norwegian Research Council of Science and Humanities for a travel grant.

Appendix A

VERTICES APPEARING IN DOUBLE-PENGUIN-LIKE DIAGRAMS

Our calculation involves the ordinary quark-gluon coupling

$$g_s(p^2)\bar{q}\gamma_\mu t^a q \tag{A.1}$$

as well as the s → dG vertex (fig. 6)

$$f_P(p^2)L_q(p^2)\,\bar{d}\gamma_\alpha t^a LsP_T(p)^\alpha_\rho\,, \tag{A.2}$$

where

$$f_P(p^2) = -\frac{\sqrt{2}\,G_F}{3}\frac{g_s(p^2)}{4\pi^2} \tag{A.3}$$

and P_T is the transverse projector

$$P_T(p)^{\alpha\beta} = p^2 g^{\alpha\beta} - p^\alpha p^\beta\,. \tag{A.4}$$

After the Wick rotation, we obtain

$$L_q(p^2) = 6\int_0^1 \mathrm{d}x\,x(1-x)\ln\frac{M_W^2(1-x)+m_q^2 x+p^2x(1-x)}{m_q^2+p^2x(1-x)}\,. \tag{A.5}$$

The analogous s → dGG vertex (fig. 8) is somewhat more complex:

$$f_T(p^2)\,\bar{d}t^b t^a\gamma^\mu T_{\mu\rho\sigma}(p^2)Ls\,, \tag{A.6}$$

where*

$$f_T(p^2) = 2\sqrt{2}\,G_F\frac{\alpha_s(p^2)}{4\pi}\,. \tag{A.7}$$

The tensor $T_{\mu\rho\sigma}$, defined by eqs. (2.16) and (2.17), is expressed through the functions

* Note that $g_s f_P = -\frac{2}{3}f_T$.

A, B, C and F. After taking the euclidean momenta we obtain

$$A(p^2, m^2) = \tfrac{1}{4} f(n) \int_0^1 \mathrm{d}x\,(1-x)\{(2-n)(1-x) I_2 + 4[x^2(1-x)p^2 + m^2(1-x)] I_3\}, \quad \text{(A.8)}$$

$$B(p^2, m^2) = \tfrac{1}{4} f(n) \int_0^1 \mathrm{d}x\,(1-x)\{-(2-n)(1+x) I_2 + 4[x^2(1-x)p^2 - m^2(1+x)] I_3\}, \quad \text{(A.9)}$$

$$C(p^2, m^2) = \tfrac{1}{4} f(n) \int_0^1 \mathrm{d}x\,(1-x) 16 x^2 (1-x) I_3, \quad \text{(A.10)}$$

$$F(p^2, m^2) = \tfrac{1}{16} f(n)[F_2 + F_3 + m^2 G], \quad \text{(A.11)}$$

where

$$F_2 = \int_0^1 \mathrm{d}x\,(1-x)\{-x(2+n) + (6-n)\} I_2,$$

$$F_3 = \int_0^1 \mathrm{d}x\,(1-x)^2 4x^2 p^2 I_3,$$

$$G = 4 \int_0^1 \mathrm{d}x\,(1-x^2) I_3,$$

$$f(n) = \mathrm{Tr}\, 1_{\mathrm{Dirac}} = 2n - 4 \to 4. \quad \text{(A.12)}$$

Finally, I_2 represents a divergent expression which, in dimensional regularization, takes a form

$$I_2 = \frac{i}{16\pi^2} \left\{ \frac{1}{2 - \frac{1}{2}n} - \gamma_{\mathrm{E}} + \ln(4\pi\nu^2) - \ln[m^2 + x(1-x)p^2] \right\}. \quad \text{(A.13)}$$

Here, the last term leads to the so-called leading logarithmic (l-log) behaviour, while the constant terms cancel by the GIM mechanism. In contrast to I_2, I_3 is the finite expression

$$I_3 = -\frac{i}{32\pi^2} \frac{1}{m^2 + x(1-x)p^2} \quad \text{(A.14)}$$

and offers no leading-log behaviour. Thus, in the l-log limit, our expressions reduce to those of ref. [31]. However, only the functions A and B contain l-log behaviour. The l-log behaviour in F_2 is only apparent since there is the cancellation of the pole for $n = 4$:

$$F_2 = \frac{i}{16\pi^2} \left\{ \tfrac{4}{3} - 2 \int_0^1 \mathrm{d}x\,(1-x)(1-3x) \ln[m^2 + x(1-x)p^2], \right.$$

and there is no l-log, due to

$$\int \mathrm{d}x\,(1-x)(1-3x) = 0.$$

Appendix B

ANALYTICAL APPROXIMATION AND THE DEMONSTRATION OF GAUGE INVARIANCE FOR THE *CP* VIOLATING INTERFERENCE TERMS ($\sim \lambda_u \lambda_t$)

The dominating *CP*-violating contributions $\sim \lambda_u \lambda_t$ are obtained when the c and t quarks are running in one penguin (or triangle) loop, and the u and t quarks are running in the remaining loop (see eqs. (2.2) and (2.21)). The main contributions to such loop integrals are obtained for loop momenta in the range $m_c^2 \leqslant p^2 \leqslant m_t^2$. Inspired by the previous work of refs. [17,18], we stick to the leading approximation which uses $m_c^2 \leqslant p^2 \leqslant m_t^2$ in the whole region. Thus one obtains

$$(L_c - L_t) \sim \ln \frac{m_t^2}{p^2}, \tag{B.1a}$$

$$(L_u - L_c) \sim \frac{m_c^2}{p^2}, \qquad \frac{m_c^2}{p^2} \ln \frac{p^2}{m_c^2}. \tag{B.1b}$$

This approximation underestimates $L_c - L_t$ for $p^2 \lesssim m_t^2$ and overestimates $L_u - L_c$ for $p^2 \gtrsim m_c^2$. In (B.1) L_q may symbolize both the $s \to dG$ and the $s \to dGG$ loop, respectively. Defining the integrals ($\alpha_s(p^2)$ is given in (2.23)):

$$R = \int_{m_c^2}^{m_t^2} dp^2 \left[\alpha_s(p^2)\right]^2 \left[\ln \frac{m_t^2}{p^2}\right] \frac{m_c^2}{p^2}, \tag{B.2a}$$

$$S = \int_{m_c^2}^{m_t^2} dp^2 \left[\alpha_s(p^2)\right]^2 \left[\ln \frac{m_t^2}{p^2}\right] \left[\frac{m_c^2}{p^2} \ln \frac{p^2}{m_c^2}\right], \tag{B.2b}$$

we obtain the expressions (2.9a)–(2.12a), where $\langle Q \rangle$ is the matrix element of the operator

$$Q = \frac{1}{16\pi^2} \left(\frac{2\sqrt{2}\, G_F}{4\pi}\right)^2 \left(\bar{d} \gamma_\mu L s\right)_{\text{colourless}}. \tag{B.3}$$

The combination (SR) in (2.12a) is due to the antisymmetric part of the triangle diagram. We observe that the gauge-dependent ($\sim \xi$) part of the SP, D and MP diagrams mutually cancel. The integrals R and S in (B.2) can be integrated logarithmically ($dp^2/p^2 = d(\ln p^2)$), and one obtains

$$R = \left(\frac{4\pi m_c}{b}\right)^2 \left\{\frac{1}{\eta} - 1 - \ln\left(\frac{1}{\eta}\right)\right\}, \tag{B.4}$$

$$S = \left(\frac{4\pi m_c}{b}\right)^2 \left[\frac{4\pi}{b\alpha_s(m_t^2)}\right]^2 \left\{(1+\eta)\ln\left(\frac{1}{\eta}\right) - 2(1-\eta)\right\}, \tag{B.5}$$

where

$$\eta \equiv \frac{\alpha_s(m_t^2)}{\alpha_s(m_c^2)} = 1 - b\frac{\alpha_s(m_t^2)}{4\pi}\ln\frac{m_t^2}{m_c^2}. \tag{B.6}$$

Numerically, (2.9a)–(2.12a) give numbers of the right order of magnitude. For the quantity $6\hat{R} \equiv 6[m_t\alpha_s(m_t^2)]^{-2}R$ which corresponds to $\hat{K}_{DP}$ defined in (2.24) and tabulated in table 2, we obtain $6\hat{R} \simeq 0.64$ (0.91) for $\alpha_s(m_c^2) = 0.5$ (0.6). Furthermore, for the ratios between the DP, SP, D and MP contributions the results are practically unchanged compared with the numerical integration result presented in the middle row of table 3,

$$\text{DP} : \text{SP} : \text{D} : \text{MP} \simeq 1 : 0.47 : (-0.52) : 2.3\ (2.4) \tag{B.7}$$

for $\alpha_s(m_c^2) \simeq 0.5$ (0.6). From (B.4)–(B.5) we observe that the contributions in (2.9a)–(2.12a) do not depend critically on m_t. The indirect dependence of μ through $\alpha_s(m_c^2)$ is more pronounced (which is also visible through the LEGO plots).

Appendix C

COLOUR FACTORS

In order to compare the standard-box contribution and various DPL contributions, we have to extract colour factors, i.e. to evaluate the colour part of the K^0 to $\bar{K}^0$ matrix element. DPL diagrams, involving the exchange of two gluons, lead to colour operators ($t^a = \frac{1}{2}\lambda^a$)

$$(t^a t^b) \otimes (t^a t^b) \qquad \text{and} \qquad (t^a t^b) \otimes (t^b t^a). \tag{C.1}$$

Using the properties of the SU(3) λ-matrices

$$\lambda^a\lambda^b = \tfrac{2}{3}\delta^{ab} + F^{abc}\lambda^c, \qquad F^{abc} = d^{abc} + if^{abc} \tag{C.2}$$

and the relations

$$d^{aab} = f^{aab} = 0, \qquad d^{abc}d^{abd} = \tfrac{5}{3}\delta^{cd}, \qquad f^{abc}f^{abd} = 3\delta^{cd}, \tag{C.3}$$

we obtain for a given diagram and its crossed counterpart, respectively,

$$(t^a t^b) \otimes (t^b t^a) = \tfrac{2}{9}1 \otimes 1 + \tfrac{1}{4}\left(\tfrac{5}{3} + 3\right)t^a \otimes t^a, \tag{C.4}$$

$$(t^a t^b) \otimes (t^a t^b) = \tfrac{2}{9}1 \otimes 1 + \tfrac{1}{4}\left(\tfrac{5}{3} - 3\right)t^a \otimes t^a. \tag{C.5}$$

Thus there are two relevant four-quark colour singlet operators for the DPL diagrams

$$Q_0 = (\bar{d}^i\gamma^\mu Ls^i)(\bar{d}^j\gamma_\mu Ls^j), \tag{C.6}$$

$$Q_1 = (\bar{d}\gamma^\mu Lt^a s)(\bar{d}\gamma_\mu Lt^a s). \tag{C.7}$$

Furthermore, the mesonic colour states $\delta^{ik}/\sqrt{3}$ and $\delta^{jl}/\sqrt{3}$ give different matrix

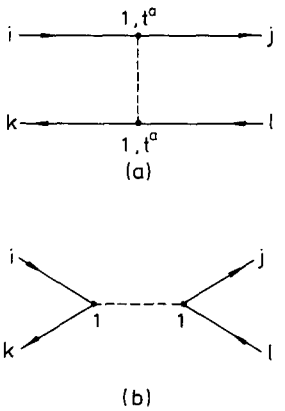

Fig. 15. Schematic presentation of the extraction of colour factors for the operators giving the K^0–$\bar{K}^0$ mixing: (a) for the scattering channel, (b) for the annihilation channel.

elements for the scattering (fig. 15a) and annihilation (fig. 15b) channels. The well-known example is the standard box containing the Q_0 operator only, for which the evaluation of the colour part yields

$$\langle Q_0 \rangle^{\text{scattering}} = (\bar{d}\gamma^\mu Ls)^2_{\text{colourless}}, \tag{C.8}$$

$$\langle Q_0 \rangle^{\text{annihilation}} = 3(\bar{d}\gamma^\mu Ls)^2_{\text{colourless}}. \tag{C.9}$$

This suppression of the scattering channel by a factor of 3 may be viewed as an $1/N_c$ correction [32] to the annihilation channel (N_c = number of colours). Similar reductions to $(\bar{d}\gamma^\mu Ls)^2 \equiv (\bar{d}\gamma^\mu Ls)^2_{\text{colourless}}$ for DPL diagrams lead to colour factors explicitly given in sect. 2.

References

[1] M.K. Gaillard and B.W. Lee, Phys. Rev. D10 (1974) 897
[2] S.L. Glashow, J. Iliopoulos and L. Maiani, Phys. Rev. D2 (1970) 1285
[3] I.I. Bigi, Z. Phys. C27 (1985) 303;
M. Gronau and J. Schechter, Phys. Rev. D31 (1984) 1668;
A.A. Anselm et al., Phys. Lett. 156B (1985) 102;
X.-G. He and S. Pakvasa, Phys. Lett. 156B (1985) 236;
U. Türke et al., Nucl. Phys. B258 (1985) 313;
T. Hayashi et al., KTCP-8502/HUPD-8511 preprint
[4] See J.-M. Frere, ULB-TH 86/06 and references therein
[5] See J.-M. Gérard, MPI-PAE/PTh 63/85 and references therein
[6] L.F. Abbott, P. Sikivie and M.B. Wise, Phys. Rev. D21 (1980) 1393;
G.G. Athanasiu and F.J. Gilman, Phys. Lett. 153B (1985) 274;
G.G. Athanasiu et al., Phys. Rev. D32 (1985) 3020;
U. Shankar, UPR-0290 T (1985) preprint

[7] K. Senba and M. Tanimoto, Phys. Lett. 150B (1985) 209;
I.I. Bigi, TRI-PP-85-19 preprint
[8] H.B. Nielsen and I. Picek, Nucl. Phys. B211 (1983) 269, (Add.) Nucl. Phys. B242 (1984) 542;
I. Picek, Phys. Lett. 159B (1985) 385
[9] L. Wolfenstein, Nucl. Phys. B160 (1979) 501;
C.T. Hill, Phys. Lett. 97B (1980) 275;
I.I. Bigi and A.I. Sanda, Phys. Lett. 148B (1984) 205;
J.F. Donoghue, E. Golowich and B.R. Holstein, Phys. Lett. 135B (1984) 481
[10] J.F. Donoghue and B.R. Holstein, Phys. Rev. D29 (1984) 2088;
J.M. Frere et al., Phys. Lett. 151B (1985) 161; see also refs. [28] and [32]
[11] J. Ellis et al., Nucl. Phys. B131 (1977) 285;
J.S. Hagelin, Nucl. Phys. B193 (1981) 123;
F.J. Gilman and J.S. Hagelin, Phys. Lett. 133B (1983) 443;
E.A. Paschos, B. Stech and U. Türke, Phys. Lett. 128B (1983) 240;
L. Wolfenstein, Nucl. Phys. B246 (1984) 45;
I.I. Bigi and A.I. Sanda, Phys. Rev. D29 (1984) 1393;
A.J. Buras, W. Slominski and H. Steger, Nucl. Phys. B238 (1984) 529, B245 (1984) 369
[12] J.F. Donoghue et al., Phys. Rev. D33 (1986) 179;
I. Picek, Fizika 18 (1986) 66
[13] UA1 collaboration, presented by K. Eggert at the XXI Recontre de Moriond (1986)
[14] D. Hochberg and R.G. Sachs, Phys. Rev. D27 (1983) 606
[15] G. Ecker, Phys. Lett. 147B (1984) 369
[16] J.N. Webb, Z. Phys. C27 (1985) 611
[17] J.O. Eeg and I. Picek, Phys. Lett. 160B (1985) 154
[18] J.O. Eeg and I. Picek, Phys. Lett. 177B (1986) 432
[19] L. Wolfenstein in ref. [9];
J.F. Donoghue, E. Golowich and B.R. Holstein, Phys. Lett. 119B (1982) 412;
A. Pich and E. de Rafael, Phys. Lett. 158B (1985) 477;
R. Decker, Univ. of Karlsruhe preprint TKP 86-1;
P. Langacker, in Proc. of the 1985 Int. Symp. on Lepton and photon interactions at high energies, ed. M. Konuma and K. Takahashi (Kyoto 1986)
[20] A. Datta and D. Kumbhakar, Phys. Rev. D33 (1986) 3461
[21] A.I. Vainshtein et al., Yad. Fiz. 23 (1976) 1024; [Sov. J. Nucl. Phys. 23 (1976) 540]; Phys. Rev. D16 (1977) 223
[22] J.O. Eeg, Phys. Rev. D23 (1981) 2596
[23] J.O. Eeg and I. Picek, Nucl. Phys. B244 (1984) 77
[24] G.P. Lepage, J. Comput. Phys. 27 (1978) 192
[25] F.J. Gilman and M.B. Wise, Phys. Lett. 93B (1980) 129; Phys. Rev. D27 (1983) 1128
[26] J.F. Donoghue, E. Golowich and B.R. Holstein, Phys. Lett. 135B (1983) 481
[27] J.F. Donoghue, E. Golowich and G. Valencia, Phys. Rev. D33 (1986) 1387
[28] J.F. Donoghue, E. Golowich and B. Holstein, Phys. Reports 131 (1986) 319
[29] R.D. Peccei, DESY report 85-121
[30] F.J. Gilman, SLAC-PUB-3951 (1986)
[31] M.B. Wise and E. Witten, Phys. Rev. D20 (1979) 1216;
E. de Rafael, MPI-PAE/PTh 72/84 report
[32] A.J. Buras and J.-M. Gérard, Nucl. Phys. B264 (1986) 371